Inorganic Chemistry

pubs.acs.org/IC

Article

Two-Electron Mixed Valency in a Heterotrimetallic Nickel−Vanadium−Nickel Complex

Michael K. Wojnar, Joseph W. Ziller, and Alan F. Heyduk*

Cite This: *Inorg. Chem.* 2023, 62, 1405−1413

Read Online

ACCESS | Metrics & More | Article Recommendations | Supporting Information

ABSTRACT: Mixed-valence complexes represent an enticing class of coordination compounds to interrogate electron transfer confined within a molecular framework. The diamagnetic heterotrimetallic anion, $[V(SNS)_2\{Ni(dppe)\}_2]^-$, was prepared by reducing $(dppe)NiCl_2$ in the presence of the chelating metalloligand $[V(SNS)_2]^-$ [dppe = bis(diphenylphosphino)ethane; $(SNS)^{3-}$ = bis(2-thiolato-4-methylphenyl)-amide]. Vanadium−nickel bonds span the heterotrimetallic core in the structure of $[V(SNS)_2\{Ni(dppe)\}_2]^-$, with V−Ni bond lengths of 2.78 and 2.79 Å. One-electron oxidation of monoanionic $[V(SNS)_2\{Ni(dppe)\}_2]^-$ yielded neutral, paramagnetic $V(SNS)_2\{Ni(dppe)\}_2$. The solid-state structure of $V(SNS)_2\{Ni(dppe)\}_2$ revealed that the two nickel ions occupy unique coordination environments: one nickel is in a square-planar S_2P_2 coordination environment (τ_4 = 0.19), with a long Ni···V distance of 3.45 Å; the other nickel is in a tetrahedral S_2P_2 coordination environment (τ_4 = 0.84) with a short Ni−V distance of 2.60 Å, consistent with a formal metal−metal bond. Continuous-wave X-band electron paramagnetic resonance spectroscopy, electrochemical investigations, and density functional theory computations indicated that the unpaired electron in the neutral $V(SNS)_2\{Ni(dppe)\}_2$ cluster is localized on the bridging $[V(SNS)_2]$ metalloligand, and as a result, $V(SNS)_2\{Ni(dppe)\}_2$ is best described as a two-electron mixed-valence complex. These results demonstrate the important role that metal−metal interactions and flexible coordination geometries play in enabling multiple, reversible electron transfer processes in small cluster complexes.

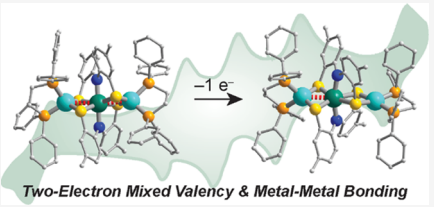

INTRODUCTION

Mixed valency is a key contributor to the electronic structure and reactivities of many metalloenzymes[1] and the unique properties inherent to magnetic[2,3] and conductive materials.[4,5] The degree of electronic delocalization within a mixed-valence system manifests novel electronic characteristics, including shifted redox potentials, enhanced magnetic exchange interactions,[6,7] and the ability to store and even transfer spin information.[8] For example, the rapid oscillation of charge between redox centers has been implicated in the semi-conducting properties of Prussian blue and the long-range electron transfer processes observed in photosynthetic and respiratory proteins.[9] The degree of electronic delocalization (or electron hopping) between redox sites often is defined by the degree of electronic communication within the Robin−Day scheme of mixed valency. In Class I (valence-trapped) complexes, the odd electron is restricted to a single redox site (M^n−M^{n+1}).[10] In Class III complexes, the odd electron is delocalized evenly over both redox sites ($M^{n+1/2}$−$M^{n+1/2}$). Class II complexes occupy the chemical space between these two extremes, where the odd electron is neither completely trapped at one redox center nor fully delocalized over both redox centers. Defining these boundaries is an ongoing challenge in the field of mixed-valence chemistry.[11−13]

Traditionally, mixed valency refers to molecular complexes or extended frameworks in which the redox centers differ by a single electron. Such one-electron mixed-valence systems provide a means to investigate the impact that reorganization energy, electronic delocalization, and thermodynamic driving force (in systems where the redox sites are different) have on intramolecular electron-transfer reactions.[14,15] Two-electron mixed-valence complexes, which are characterized by redox centers that differ by two electrons, while less well developed, have attracted attention for their potential roles in promoting multi-electron reactivity.[16,17] Two-electron mixed-valence dirhodium and diiridium complexes with a metal−metal bond have been utilized in photochemical strategies for splitting hydrohalic acids,[18−30] whereas two-electron mixed-valence intermediates have been implicated in the reactivity of biomimetic iron−nickel hydrogenase model complexes.[31,32] Often, two-electron mixed-valence complexes are characterized by redox centers that have metal ions with different coordination numbers and in distinctly different coordination geometries. For example, the two-electron mixed-valence dirhodium complexes comprise six-coordinate octahedral rhodium(II) centers and five-coordinate trigonal bipyramidal rhodium(0) centers.[33] Similarly, two-electron mixed-valence

Received: September 28, 2022
Published: January 12, 2023

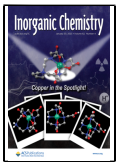

https://doi.org/10.1021/acs.inorgchem.2c03381
Inorg. Chem. 2023, 62, 1405−1413

iridium phosphine complexes have six-coordinate octahedral iridium(II) centers and four-coordinate iridium(0) centers.[28]

Herein, we report the synthesis of the neutral heterotrimetallic cluster complex, $V(SNS)_2\{Ni(dppe)\}_2$, and the corresponding one-electron-reduced anion, $[V(SNS)_2\{Ni(dppe)\}_2]^-$. Examination of these closely related complexes revealed dramatic and reversible structural and electronic changes within a multimetallic core upon removal of a single redox equivalent. The anionic complex is best described as a symmetric $[Ni^0–V^V–Ni^0]^{1-}$ anion with short Ni–V interactions across the heterotrimetallic core. Removal of a single electron afforded the neutral complex, best described as a two-electron mixed-valence species, with a $Ni^0–V^{IV}\cdots Ni^{II}$ core in which a short Ni–V interaction is only observed for the reduced nickel center. The new complexes were characterized by single-crystal X-ray crystallography, electron paramagnetic resonance (EPR) spectroscopy, and cyclic voltammetry. These clusters illustrate how changes in coordination geometry and metal–metal interactions work to accommodate changes to the valence electron count of a heterotrimetallic core.

RESULTS

Synthesis and Structural Characterization. The new vanadium metalloligand $[V(SNS)_2]^{1-}$ was prepared by salt metathesis, similar to the previously reported tungsten derivative.[34] Treatment of $(SNS)H_3$ with three equivalents of potassium hydride resulted in the deprotonation of both the thiophenol and amine groups of the proligand. The resulting tribasic salt was then combined with $VCl_3(THF)_3$ and the two-electron oxidant $PhICl_2$ in a 2:1:1 ratio as shown in Scheme 1

Scheme 1

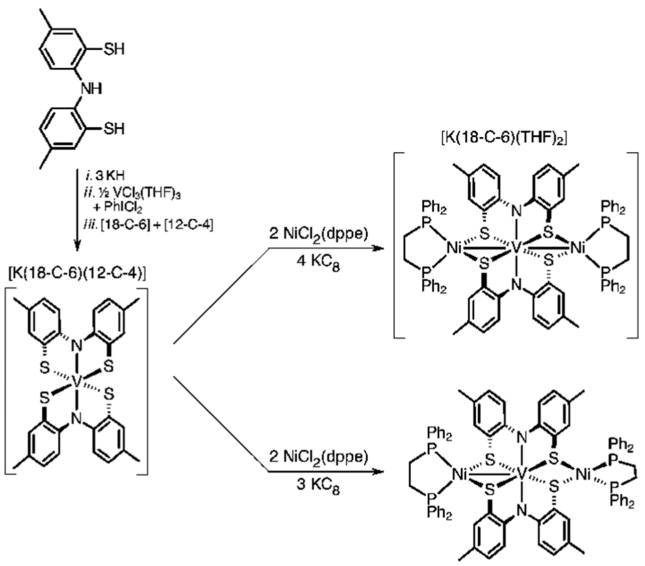

(THF = tetrahydrofuran) . Aerobic workup of the reaction mixture afforded the desired vanadate anion as the potassium salt in 70% yield as a dark-blue solid. Attempts to access the homoleptic anion from VCl_5 yielded intractable product mixtures. The presence of $[V(SNS)_2]^{1-}$ was confirmed by a parent ion peak in the negative-mode electrospray mass spectrum at m/z = 567.1 amu. The ^1H NMR spectrum was consistent with nominal C_{2v} symmetry for the diamagnetic complex.

In a strongly reducing environment, the anionic metalloligand $[V(SNS)_2]^{1-}$ readily reacted with two equivalents of $NiCl_2(dppe)$ to afford trimetallic cluster complexes. The reaction of one equivalent of $K[V(SNS)_2]$ with two equivalents of $NiCl_2(dppe)$ and four equivalents of KC_8 afforded a dark-green complex characterized as $[K(18\text{-crown-6})(THF)_2][V(SNS)_2\{Ni(dppe)\}_2]^{1-}$, Scheme 1. The formation of the trimetallic anion was indicated by a parent ion peak at m/z = 1479.2 amu in the negative-mode electrospray mass spectrum. ^1H and $^{31}P\{^1H\}$ NMR data at 208 K indicate a symmetric diamagnetic species with a 1:2 ratio of $[V(SNS)_2]^{1-}$ to Ni(dppe) fragments. When the same reaction was carried out with only three equivalents of KC_8, a paramagnetic product was obtained. Again, the formation of the trimetallic cluster was indicated by mass spectrometry, this time by an M+1 peak at m/z = 1480.2 amu in the positive-mode electrospray mass spectrum. This paramagnetic product was assigned as the neutral complex, $V(SNS)_2\{Ni(dppe)\}_2$, as illustrated in Scheme 1. Accordingly, electronic absorption spectra of $[V(SNS)_2]^{1-}$ and $V(SNS)_2\{Ni(dppe)\}_2$ in THF were obtained and demonstrated two prominent transitions at 350–400 nm and at ~630 nm (Figures S23 and S24). It is notable that the ultraviolet–visible–near-infrared (UV–vis–NIR) spectra for both neutral $V(SNS)_2\{Ni(dppe)\}_2$ and anionic $[V(SNS)_2\{Ni(dppe)\}_2]^{1-}$ show no discernible absorption bands in the low-energy region (900–1400 nm).

Single-crystal X-ray diffraction experiments were used to establish the molecular geometry of the new coordination complexes, including the $[V(SNS)_2]^{1-}$ metalloligand. The vanadium metalloligand itself crystallized with a [K(18-crown-6) (12-crown-4)] countercation in the monoclinic space group, $P2_1n$. An *Oak Ridge thermal-ellipsoid plot* (ORTEP) of the $[V(SNS)_2]^{1-}$ anion and selected metrical parameters from the structure are available in the Supporting Information. The vanadium center of the anion is six-coordinate with a *pseudo*-octahedral geometry as defined by a Bailar twist angle of 45° and 'trans' X–V–X bond angles of approximately 158° (X = N or S). The V–S and V–N bond distances are normal for vanadium(V)–thiolate and vanadium(V)–azanido interactions, and bond distances within the ligand backbone are consistent with the fully reduced $(SNS)^{3-}$ oxidation state.[35–41]

Single-crystal X-ray diffraction was used to interrogate the structure of the heterotrimetallic Ni–V–Ni clusters. The salt of the heterotrimetallic anion crystallized in the monoclinic $P2_1c$ space group by slow diffusion of pentane into a saturated solution of the complex in THF. The potassium cation of the salt was sequestered from the heterotrimetallic anion with 18-crown-6 and two THF ligands. As shown in Figure 1 (left), the structure of the $[V(SNS)_2\{Ni(dppe)\}_2]^{1-}$ anion comprises a *pseudo*-octahedral vanadium unit sandwiched by two *pseudo*-tetrahedral nickel fragments with Ni τ_4 values of 0.86 and 0.81 (assigned geometries do not include the metal–metal interactions). Selected metrical data for $[K(18\text{-crown-6})(THF)_2][V(SNS)_2\{Ni(dppe)\}_2]$ are given in Figure 2. Nickel–vanadium distances, which are each bridged by two thiolates from the $(SNS)^{3-}$ ligands, are relatively short at 2.78 and 2.79 Å. These values are in the order of the sum of the covalent radii of vanadium and nickel (2.77 Å), with covalent ratios (r) of 1.00 and 1.01.[42,43] Although there is a paucity of vanadium–nickel metal–metal bonds in the literature,[44–46] these distances are consistent with a formal bonding interaction between the metal centers. The bridging nature of the thiolates results in a slight elongation of the vanadium–

https://doi.org/10.1021/acs.inorgchem.2c03381
Inorg. Chem. 2023, 62, 1405–1413

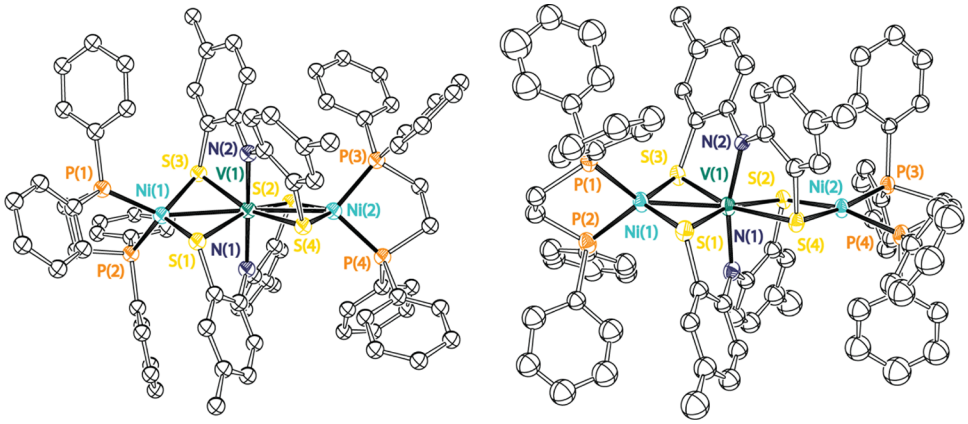

Figure 1. ORTEPs of (left) [K(18-crown-6) $(THF)_2$][$V(SNS)_2${Ni(dppe)}$_2$] and (right) $V(SNS)_2${Ni(dppe)}$_2$ with thermal ellipsoids shown at 50% probability. Hydrogen atoms, solvent molecules, and counterions have been omitted for clarity.

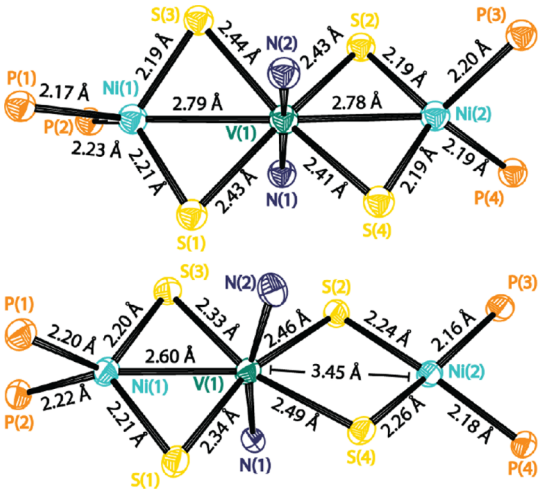

Figure 2. ORTEP of trimetallic cores of (top) anionic [$V(SNS)_2${Ni(dppe)}$_2$]$^{1-}$ and (bottom) neutral $V(SNS)_2${Ni(dppe)}$_2$ with thermal ellipsoids shown at 50% probability. A full list of bond distances and angles is included in the Supporting Information.

sulfur distance from V−S_{avg} = 2.36 Å in the free [$V(SNS)_2$]$^{1-}$ anion to V−S_{avg} = 2.43 Å in the [$V(SNS)_2${Ni(dppe)}$_2$]$^{1-}$ trimetallic cluster. The nickel−sulfur and nickel−phosphorous distances are consistent with those of other low-valent nickel complexes in the literature.[32,47]

In contrast with the symmetric structure observed for the [$V(SNS)_2${Ni(dppe)}$_2$]$^{1-}$ anion, the neutral $V(SNS)_2${Ni(dppe)}$_2$ complex shows distinctly different geometries at the two nickel centers. For the neutral complex, $V(SNS)_2${Ni(dppe)}$_2$, X-ray-quality single crystals were obtained in the orthorhombic $Pna2_1$ space group by allowing pentane to diffuse into a concentrated THF solution of the complex. Figure 1 (right) shows an ORTEP of the neutral $V(SNS)_2${Ni(dppe)}$_2$ complex, and Table S4 gives selected metrical parameters for the trimetallic cluster. While the vanadium center remains *pseudo*-octahedral and sandwiched between the two nickel centers of the trimetallic cluster, one nickel adopts a *pseudo*-tetrahedral geometry with a τ_4 value of 0.84, and the second nickel adopts a *pseudo*-square-planar geometry with a τ_4 value of 0.19. A short V−Ni distance of 2.60 Å is maintained between the vanadium and the tetrahedral nickel (r = 0.94) and is indicative of a metal−metal bond; conversely, a V···Ni distance of 3.45 Å between the vanadium and the square-planar nickel is too long for a formal metal−metal bond (r = 1.25) (Figure 2). The nitrogen atoms of each SNS ligand bend toward the sterically less-constrained square-planar nickel center, evidenced by a N−V−Ni bond angle of 164.36° (the N−V−Ni bond angle in the anion is 171.95°). The square-planar nickel center is further differentiated by elongated Ni−S bonds and slightly contracted Ni−P bonds, which are consistent with distances for nickel(II) complexes reported in the literature.[48−50]

EPR Spectroscopy. The neutral heterotrimetallic cluster $V(SNS)_2${Ni(dppe)}$_2$ is an odd-electron, paramagnetic species and was probed via continuous-wave (cw) X-band EPR spectroscopy to determine the magnitude and localization of the unpaired spin density. Figure 3 (bottom) displays the EPR

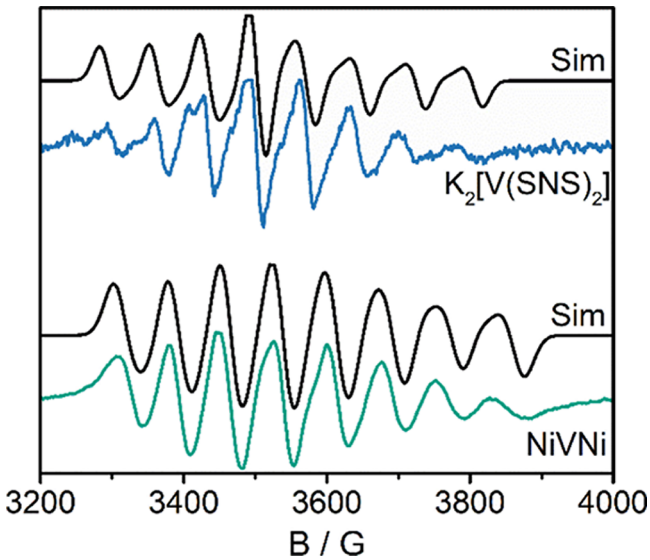

Figure 3. Solution cw X-band EPR spectra in THF of (top) in situ-prepared [$V(SNS)_2$]$^{2-}$ and (bottom) $V(SNS)_2${Ni(dppe)}$_2$ at 298 K.

spectrum obtained for the complex in THF at 298 K and demonstrates that $V(SNS)_2${Ni(dppe)}$_2$ is an S = 1/2 complex. At 298 K, the EPR spectrum exhibits an eight-line signal spread over ∼1000 G, consistent with an electron−nuclear hyperfine interaction of the unpaired electron with the vanadium center (I = 7/2 for ^{51}V nuclei). The spectrum was simulated in EASYSPIN using the spin Hamiltonian

https://doi.org/10.1021/acs.inorgchem.2c03381
Inorg. Chem. 2023, 62, 1405−1413

$$\hat{H} = g\mu_B \boldsymbol{BS} + \boldsymbol{IAS}$$

where g is the g-factor, μ_B the Bohr magneton, $\boldsymbol{B}$ the magnetic field, $\boldsymbol{S}$ the electronic spin, $\boldsymbol{I}$ the nuclear spin of the metal nucleus, and $\boldsymbol{A}$ the rhombic hyperfine coupling. The best simulations of $V(SNS)_2\{Ni(dppe)\}_2$ at 298 K used an $S = 1/2$ axial model with $g_\perp = 1.952$ and $g_\parallel = 1.958$ and V hyperfine coupling constants of $A_\perp = 217$ MHz and $A_\parallel = 175$ MHz. At 77 K, the signal becomes rhombic, with the frozen THF solution spectrum of $V(SNS)_2\{Ni(dppe)\}_2$ displaying the eight-line electron−nuclear hyperfine with a rhombic signal centered at $g = 1.95$ (Table 1; Figure S22). To benchmark the

Table 1. Spin Hamiltonian Parameters for $V(SNS)_2\{Ni(dppe)\}_2$ and $K_2[V(SNS)_2]$ Obtained in THF

		$K_2[V(SNS)_2]$	$V(SNS)_2\{Ni(dppe)\}2$
298 K	g_x	1.990	1.952
	g_y	2.010	1.958
	g_z	2.010	1.958
	g_{iso}	2.003	1.956
	A_x (MHz)	422	217
	A_y (MHz)	118	175
	A_z (MHz)	118	175
	A_{iso} (MHz)	243	189
77 K	g_x	1.963	1.954
	g_y	1.981	1.960
	g_z	1.983	1.938
	g_{iso}	1.976	1.951
	A_x (MHz)	407	338
	A_y (MHz)	125	157
	A_z (MHz)	18	84
	A_{iso} (MHz)	183	193

EPR spectra of this neutral $V(SNS)_2\{Ni(dppe)\}_2$ complex, X-band EPR spectra were obtained for THF solutions of $[V(SNS)_2]^{2-}$ generated in situ by the reduction of the $[V(SNS)_2]^{1-}$ anion with KC_8. The EPR spectrum of $[V(SNS)_2]^{2-}$ at 298 K along with the simulation is displayed at the top of Figure 3. The 77 K spectrum and associated simulation are included in the Supporting Information. As expected, an eight-line, $S = 1/2$ signal was observed for putative $[V(SNS)_2]^{2-}$ at 298 K, consistent with the formation of a vanadium(IV) species. The 298 K spectrum was simulated as an axial system with larger g values and hyperfine coupling constants than those that were observed in the trimetallic complex. The 77 K spectrum of the putative dianion was rhombic, with g values and hyperfine coupling constants similar to those observed in the low-temperature spectrum of the $V(SNS)_2\{Ni(dppe)\}_2$ complex. The EPR spectra of both $V(SNS)_2\{Ni(dppe)\}_2$ and putative $[V(SNS)_2]^{2-}$ are consistent with the EPR data reported in the literature for six-coordinate vanadium(IV) complexes in sulfur-rich ligand environments.[S1−S3]

Electrochemical Analysis. Solution-phase electrochemical experiments were performed to probe the redox properties of both the $[V(SNS)_2]^{1-}$ metalloligand and the heterotrimetallic $[V(SNS)_2\{Ni(dppe)\}_2]^n$ ($n = -1, 0$) complexes. Figure 4 (top) shows the cyclic voltammogram for the $[V(SNS)_2]^{1-}$ metalloligand, whereas Figure 4 (bottom) shows the cyclic voltammogram for the neutral $V(SNS)_2\{Ni(dppe)\}_2$ complex. Cyclic voltammograms for the $[V(SNS)_2\{Ni(dppe)\}_2]^{1-}$ anion were identical to those for the neutral complex, save for the

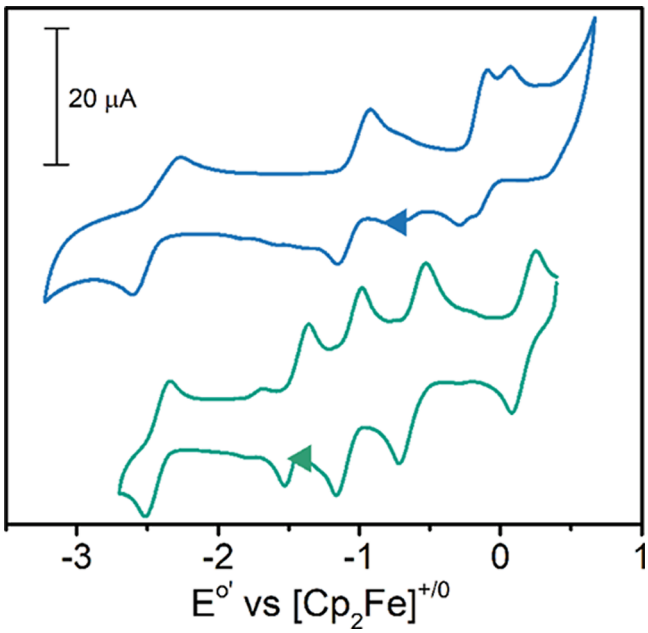

Figure 4. Cyclic voltammograms of (top, blue) $[V(SNS)_2]^{1-}$ and (bottom, green) $V(SNS)_2\{Ni(dppe)\}_2$ in THF containing 0.1 M $[Bu_4N][PF_6]$, referenced to $[Cp_2Fe]^{+/0}$. Data were collected using a glassy carbon working electrode and a 200 mV s^{-1} scan rate. The arrow denotes the open-circuit potential and the direction of the scan.

shift in the open-circuit potential and a slight change in potentials due to charge. All electrochemical experiments were conducted on THF solutions at ambient glovebox temperature using a standard three-electrode cell and 0.1 M $[Bu_4N][PF_6]$ as the supporting electrolyte. Electrochemical cell potentials, which are collected in Table 2, were referenced to $[Cp_2Fe]^{+/0}$ by the addition of an internal standard at the end of each experiment.

The vanadium metalloligand, $[V(SNS)_2]^{1-}$, shows four redox processes between −3 and +0.5 V versus $[Cp_2Fe]^{+/0}$. Two quasi-reversible reductions were observed at −0.99 and at −2.43 V ($i_{pa}/i_{pc} \sim 1$), consistent with metal-centered reductions to generate formal vanadium(IV) and vanadium(III) species, respectively. At less negative potentials (between −0.5 and 0 V), two closely spaced redox processes were observed corresponding to oxidations of the $[V(SNS)_2]^{1-}$ anion. These oxidations are assigned as ligand-centered oxidations that generate a semi-quinonate oxidation state, $(SNS^{\cdot})^{2-}$.[S4] The small separation between these oxidations suggests that the two ligands show limited electronic communication ($K_c = 72$).

For the neutral trimetallic $V(SNS)_2\{Ni(dppe)\}_2$ complex, five quasi-reversible redox processes are observed in the −3.0−+0.5 V window. The open-circuit potential for the neutral complex was determined to be near −1.2 V, and as such, the redox processes observed at −1.44 and −2.42 V are assigned as one-electron reductions, whereas the redox processes at −1.06, −0.62, and +0.17 V are assigned as one-electron oxidations. These assignments are consistent with the cyclic voltammogram of the heterotrimetallic anion, $[V(SNS)_2\{Ni(dppe)\}_2]^{1-}$, which shows the same five redox processes, but the open-circuit potential shifts to approximately −1.9 V. Based on this electrochemical data, the redox process at −1.44 V corresponds to the reduction of $V(SNS)_2\{Ni(dppe)\}_2$ to the $[V(SNS)_2\{Ni(dppe)\}_2]^{1-}$ anion. Accordingly, chemical redox

https://doi.org/10.1021/acs.inorgchem.2c03381
Inorg. Chem. 2023, 62, 1405−1413

Table 2. Electrochemical Cell Potentials (V) in THF of $K[V(SNS)_2]$ and $V(SNS)_2\{Ni(dppe)\}_2$, Referenced to $[Cp_2Fe]^{+/0}$[a]

	$[M]^{-1/-2}$	$[M]^{0/-1}$	$[M]^{+1/0}$	$[M]^{+2/+1}$	$[M]^{+3/+2}$
$K[V(SNS)_2]$	−2.43	−0.99	−0.16	−0.05	
$V(SNS)_2\{Ni(dppe)\}_2$	−2.42	−1.44	−1.06	−0.62	+0.17

[a][M] is used to denote the entire complex, not an individual metal center.

reactions can be used to convert between the neutral and anionic trimetallic complexes. For example, the addition of $CoCp^*_2$ to paramagnetic $V(SNS)_2\{Ni(dppe)\}_2$ readily produced $[V(SNS)_2\{Ni(dppe)\}_2]^{1-}$, which was observed by ^1H NMR spectroscopy. Tentative assignments for all five redox waves are provided in the Discussion section.

DFT Computations. To further analyze the electronic structure of the neutral heterotrimetallic $V(SNS)_2\{Ni(dppe)\}_2$ complex, gas-phase density functional theory (DFT) calculations were carried out using the non-empirical *tpss* functional as employed in TURBOMOLE. We modeled $V(SNS)_2\{Ni(dppe)\}_2$ as an open-shell doublet via a Kohn−Sham DFT solution, using a spin-unrestricted (unrestricted Hartree−Fock, UHF) scheme. The calculations refined and converged normally. The metal−heteroatom bond distances were within 0.04 Å of the experimental solid-state structure. Metal−metal bond distances were calculated to be 2.528 and 3.556 Å, which are markedly different than the experimental values for the tetrahedral and square-planar nickel centers, respectively, which has been observed in DFT calculations of other vanadium−nickel heterobimetallic complexes.[46] According to Mulliken population analysis (MPA) of the singly occupied molecular orbital (SOMO) of $V(SNS)_2\{Ni(dppe)\}_2$, the unpaired electron is localized on the vanadium metalloligand bridge, with small Ni(dppe) ion contributions of 1% each (Figure 5).

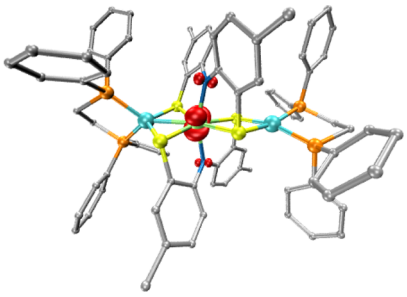

Figure 5. Kohn−Sham SOMO of $V(SNS)_2\{Ni(dppe)\}_2$ with isovalues 0.1, as determined by DFT computations at the tpss/def2-TZVP level of theory.

DISCUSSION

Homoleptic transition metal complexes of the trianionic $(ONO)^{3-}$ and $(SNS)^{3-}$ ligands have emerged as useful building blocks for the synthesis of bi- and trimetallic cluster complexes.[54−57] Previously, we reported the synthesis of several heterobimetallic complexes of the formula $M(SNS)_2M'(dppe)$ (M = Mo, M' = Ni; M = W, M' = Ni, Pd, Pt), of which the $W(SNS)_2Ni(dppe)$ derivative proved to be a catalyst for the electrochemical reduction of protons to hydrogen in non-aqueous solution.[56] We also reported the synthesis of the symmetric, heterotrimetallic $Mo(SNS)_2\{Ni(dppe)\}_2$ complex, which showed a rich redox manifold, with five reversible one-electron redox processes.[54] The nature of these redox processes and the symmetry of the heterotrimetallic complex suggested the generation of a mixed-valence species upon formation of the one-electron oxidized $[Mo(SNS)_2\{Ni(dppe)\}_2]^{1+}$ cation. To better understand the nature of this putative mixed-valence trimetallic platform, we sought to prepare isostructural and isoelectronic complexes for further study.

The vanadium anion, $[V(SNS)_2]^{1-}$, was targeted as a potential metalloligand, analogous to the neutral $Mo(SNS)_2$ metalloligand. From a valence electron perspective, $[V(SNS)_2]^{1-}$ is isoelectronic with $Mo(SNS)_2$, as both complexes have a d^0 electron configuration at the metal. Accordingly, the heterotrimetallic anion, $[V(SNS)_2\{Ni(dppe)\}_2]^{1-}$, is isoelectronic with neutral $Mo(SNS)_2\{Ni(dppe)\}_2$, and as such, the vanadium congener adopts the same symmetric molecular structure. Ignoring all metal−metal interactions, the heterotrimetallic anion is characterized by two *pseudo*-tetrahedral nickel centers and a *pseudo*-octahedral vanadium center. Short Ni−V distances are indicative of metal−metal bonding; however, it is important to note that from a symmetry perspective, the nickel centers compete for the same vanadium d orbital (d_{xy}, according to DFT computations). This sharing of the vanadium d_{xy} orbital can be represented as two resonance structures to describe the heterotrimetallic anion as shown in Figure 6 (top). Within this framework, the most

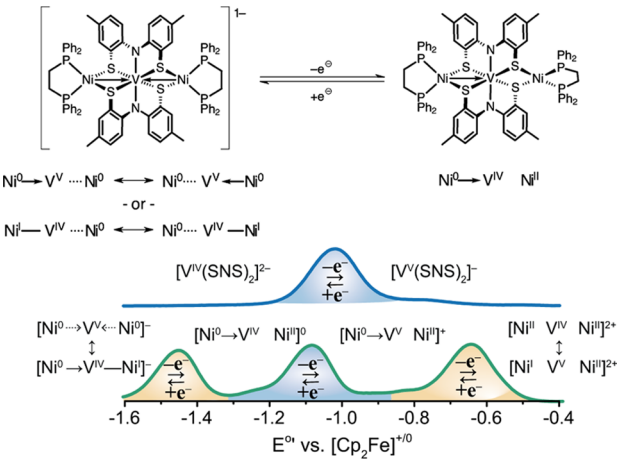

Figure 6. (Top) Scheme denoting formal oxidation state assignments for $[V(SNS)_2Ni(dppe)\}_2]^{0/+}$ and (bottom) overlay of differential pulse voltammograms of $V(SNS)_2\{Ni(dppe)\}_2$ (green) and $[V(SNS)_2]^{2-}$ (blue) in THF, denoting the locality of the redox couples [nickel (orange); vanadium (blue)].

straightforward oxidation state assignment for $[V(SNS)_2\{Ni(dppe)\}_2]^{1-}$ is $[Ni^0-V^V-Ni^0]^{1-}$, with a single $Ni^0 \rightarrow V^V$ dative bond delocalized over two equivalent positions. Alternatively, assigning one electron from the metal−metal bond to each participating metal center would afford a formal $Ni^I-V^{IV}-Ni^0$ oxidation state assignment and avoid characterizing the metal−metal bond as a dative interaction; however, the orbital

https://doi.org/10.1021/acs.inorgchem.2c03381
Inorg. Chem. 2023, 62, 1405−1413

considerations still constrain the system to a single Ni−V bond delocalized over both positions.

The solid-state structure of the neutral $V(SNS)_2\{Ni(dppe)\}_2$ complex revealed that a significant structural change accompanied the removal of an electron from the heterotrimetallic core. Removal of just one electron from the trimetallic complex induces one of the nickel centers to change from *pseudo*-tetrahedral geometry to *pseudo*-square-planar geometry. Concomitant with this geometry change is a lengthening of the nickel−vanadium distance to the square-planar nickel atom to over 3.4 Å, which is well outside the distance expected for a formal bond between these two metal atoms. Rearrangement of one nickel center to square-planar in the neutral heterotrimetallic complex also results in a contraction of nearly 0.2 Å in the distance between the remaining tetrahedral nickel and the vanadium. This contraction occurs since the participating vanadium d orbital only interacts with one nickel center.

Examination of the structural, EPR spectroscopic, and electrochemical features of the neutral $V(SNS)_2\{Ni(dppe)\}_2$ complex provides insights into its valence electron configuration. Square-planar geometry is highly correlated with the d^8 electron configuration, and as such, the square-planar nickel center can confidently be assigned to a nickel(II) oxidation state. The solution EPR data for $V(SNS)_2\{Ni(dppe)\}_2$ at both 298 and at 77 K are consistent with the presence of a single unpaired electron localized on the vanadium metalloligand. The similarity of both the EPR line position and shape to those of in situ-generated $[V(SNS)_2]^{2-}$ is highly indicative of the vanadium(IV) oxidation state. This assignment is further supported by the electrochemical data for $V(SNS)_2\{Ni(dppe)\}_2$, in which the first oxidation at −1.06 V correlates well with the $[V(SNS)_2]^{1-/2-}$ redox process at −0.99 V that is assigned as a reduction of the metal center from vanadium(V) to vanadium(IV) (Figure 6, bottom). The assignment of d^8 nickel(II) and d^1 vanadium(IV) oxidation states dictates that the remaining tetrahedral nickel center be assigned as a d^{10} nickel(0) and the attendant nickel−vanadium bond as a dative interaction, $Ni^0 \rightarrow V^{IV}$. Accordingly, the neutral, heterotrimetallic complex has a two-electron mixed-valence core, $Ni^0 \rightarrow V^{IV}{\cdots}Ni^{II}$. The two-electron mixed-valent core of the heterotrimetallic $V(SNS)_2\{Ni(dppe)\}_2$ complex is indicative of distinctly different redox potentials of the nickel centers of the complex.

Given that the first oxidation of neutral $V(SNS)_2\{Ni(dppe)\}_2$ at −1.06 V can be reasonably assigned as a vanadium-centered process, the flanking processes at −1.4 and −0.6 V then are assigned as nickel-centered redox processes. The more negative potential coincides with the conversion of neutral $V(SNS)_2\{Ni(dppe)\}_2$ to the fully characterized and symmetric anion $[V(SNS)_2\{Ni(dppe)\}_2]^{1-}$. As illustrated in Figure 6 (bottom), this redox process corresponds to the reduction of the square-planar nickel(II) center. The attendant one-electron reduction results in an intramolecular electron transfer of the unpaired electron on vanadium(IV) to the nickel center to affect the net two-electron reduction to nickel(0). This net two-electron reduction of nickel demonstrates how the vanadium metalloligand acts as a redox gate for the nickel ions: one-electron reduction of the $V(SNS)_2\{Ni(dppe)\}_2$ complex is coupled to both the intramolecular electron transfer and to a coordination geometry change from square-planar to tetrahedral to accommodate the change from nickel(II) to nickel(0). Typically, diphosphine complexes of nickel show high reorganization energies for redox processes,[47] so it is noteworthy that the redox event at −1.4 V is quasi-reversible, which in this case means that the structural changes that typically impose these high reorganization energies are instead facile on the electrochemical timescale. This dynamic and electrochemically reversible behavior has been observed in other mono-[58] and multimetallic[47,59,60] complexes containing a Ni(diphosphine) synthon.

While the cluster can store multiple reducing equivalents, several oxidizing equivalents can be stored as well. The redox process at −0.6 V is tentatively assigned as the oxidation of the tetrahedral nickel(0) center in the mixed-valent $V(SNS)_2\{Ni(dppe)\}_2$ complex. Although further studies are required to confirm the electron distribution of the $[V(SNS)_2\{Ni(dppe)\}_2]^+$ cation and the nature of its subsequent oxidation at −0.6 V, it stands to reason that this oxidation will occur at the low-valent nickel, meaning that the redox potentials for the two nickel centers, with identical S_2P_2 donor ligand sets, are separated by more than 800 mV. In this case, the large difference in redox potentials arises from the structural flexibility engendered by the $(SNS)^{3-}$ and dppe ligand platforms and the ability to make and break metal−metal bonds.

CONCLUSIONS

A pair of cluster compounds was synthesized that differ by a single electron, leading to the generation of a formally mixed-valence molecule. Neutral $V(SNS)_2\{Ni(dppe)\}_2$ contains two nickel ions in identical S_2P_2 ligand environments but in different oxidation states. Analysis of the spectroscopic, electrochemical, and structural data suggests that $V(SNS)_2\{Ni(dppe)\}_2$ is best classified as a two-electron mixed-valence system. The coordinative flexibility of the heterotrimetallic ligand framework combined with the ability of the nickel and vanadium metal centers to break and form metal−metal bonds engenders reversible redox chemistry across multiple valence electron configurations and metal oxidation states. Insights gained from these complexes are reminiscent of multimetallic metalloenzyme active sites, such as the FeNi hydrogenase or the FeMo or FeV cofactors found in nitrogenase.[61] Moreover, the heterotrimetallic complexes described demonstrate structural similarities to extended bulk materials, such as vanadium sulfide, VS_4, in the patronite mineral structure, which has exhibited metal−metal bonding throughout the extended linear chain structure as electrons are charged/discharged from the system.[62]

EXPERIMENTAL SECTION

General Considerations. All compounds and reactions reported herein show varied degrees of air and moisture sensitivity, so all manipulations were carried out using standard vacuum-line, Schlenk-line, and glovebox techniques. Solvents were sparged with argon before being deoxygenated and dried by passage through Q5 and activated alumina columns, respectively. To test for effective oxygen and water removal, aliquots of each solvent were treated with a few drops of a purple solution of the sodium benzophenone ketyl radical in THF. Commercially available reagents, including 1,2-bis(diphenylphosphino)ethane (dppe, >97%, TCI), were reagent-grade or better and used as received. The known compounds $(SNS)H_3$, $VCl_3(THF)_3$, and $NiCl_2(dppe)$ were synthesized from commercially available reagents according to procedures published in the literature.[34,63,64] Ferrocene was purified by sublimation under reduced

https://doi.org/10.1021/acs.inorgchem.2c03381
Inorg. Chem. 2023, 62, 1405−1413

pressure, and tetrabutylammonium hexafluorophosphate (Acros) was recrystallized from ethanol three times and dried under vacuum.

Spectroscopic Measurements. NMR spectra were collected at 298 K on a Bruker Avance 400 or 500 MHz spectrometer in dry, degassed CD_3CN or at 208 K in THF-d_8. ^1H NMR spectra were referenced to tetramethylsilane (TMS) using the residual proteo impurities of the given solvent. All chemical shifts are reported using the standard δ notation in parts per million; positive chemical shifts are to a higher frequency from the given reference. Electronic absorption spectra were recorded with a Jasco V-670 absorption UV-vis-NIR spectrophotometer using 1 cm path-length cells at ambient temperature (20−24 °C). Perpendicular-mode X-band EPR spectra were collected using a Bruker EMX spectrometer equipped with an ER041XG microwave bridge using the following spectrometer settings: attenuation = 20 dB, microwave power = 2.017 mW, frequency = 9.79 GHz, modulation amplitude = 1.02 G, gain = 2.00 × 103, conversion time = 81.92 ms, time constant = 655.36 ms, sweep width = 300 G, and resolution = 1024 points. The EPR spectra were modeled using EasySpin/MatLab.

Electrochemical Methods. Electrochemical experiments were performed with a Gamry Series G300 potentiostat/galvanostat/ZRA (Gamry Instruments, Warminster, PA) using a 3.0 mm glassy carbon working electrode, a platinum wire auxiliary electrode, and a silver wire pseudo-reference electrode. Data acquisition was carried out at ambient temperature (20−24 °C) in a nitrogen-filled glovebox for solution samples containing a 1.0 mM analyte and 100 mM $[Bu_4N][PF_6]$ supporting electrolyte dissolved in dry, degassed THF. All potentials were referenced to the $[Cp_2Fe]^{+/0}$ redox couple by adding ferrocene as an internal standard at the end of each experimental run.

Crystallographic Methods. X-ray diffraction data for all complexes were collected on single crystals mounted on a glass fiber using Paratone oil. Data was acquired with a Bruker SMART APEX II diffractometer equipped with a charge-coupled device detector cooled to 88 K and using Mo Kα radiation (λ = 0.71073 Å). The SMART program package was used to determine unit-cell parameters and for data collection. Raw frame data were processed using SAINT and SADABS to yield the reflection data file. Subsequent calculations were carried out using the SHELXTL program suite. The structures were solved by direct methods and refined on F^2 using full-matrix least-squares techniques. Analytical scattering factors for neutral atoms were used throughout the analyses. Hydrogen atoms were generated at calculated positions and refined using a riding model. ORTEPs were generated using ORTEP-3 for Windows.

Computational Methods. All DFT calculations were performed using the non-empirical *tpss* functional as employed in the quantum chemistry program package TURBOMOLE. For computational efficiency, initial geometry optimizations were performed using split-valence plus polarization basis sets (def2-SVP). Subsequent structural refinements and single-point energy calculations were done using a triple zeta valence plus polarization basis set (def2-TZVP). Single-crystal X-ray diffraction data were used as the starting points for geometry optimizations; no molecular symmetry was imposed. Energies and minimum energy structures were evaluated self-consistently to tighten convergence criteria (energy converged to 0.1 μHartree, maximum norm of the Cartesian gradient $\leq 10^{-4}$). Linear-response, time-dependent DFT was used to simulate electronic absorption spectra.

Synthesis of K[V(SNS)$_2$]. Solid potassium hydride (159 mg, 3.97 mmol, 6.05 equiv) was added to a chilled solution of $(SNS)H_3$ (343 mg, 1.31 mmol, 2.00 equiv) dissolved in THF, frozen in a dry ice/acetone bath, and thawed in a 100 mL Schlenk flask under an inert nitrogen atmosphere. The mixture was stirred as it warmed to ambient temperature, affording a golden−yellow, turbid mixture. Solid $VCl_3(THF)_3$ (245 mg, 0.660 mmol, 1.00 equiv) and $PhICl_2$ (180 mg, 0.660 mmol, 1.00 equiv) were added using separate solid addition funnels to yield a dark but homogeneous blue−green solution. After stirring for approximately 15 min, the reaction mixture was exposed to air, yielding a dark-blue reaction mixture, which was stirred for an additional 12 h. The reaction mixture was filtered through a plug of Celite, and then, the solvent was removed from the filtrate under reduced pressure. The remaining residue was suspended in diethyl ether, filtered, washed with another aliquot of diethyl ether, and dried under reduced pressure to afford 280 mg of a dark-blue solid (70% yield). Single crystals of the product, suitable for X-ray diffraction experiments, were obtained by allowing pentane to diffuse into a THF solution of the product and 18-crown-6. ^1H NMR (400 MHz; CD_3CN): δ/ppm: 2.35 (s, 12H, CH_3), 6.72 (d, $^3J_{HH}$ = 8.40 Hz, 4H, aryl−H), 6.92 (s, 4H, aryl−H), 7.17 (d, $^3J_{HH}$ = 8.48 Hz, 4H, aryl−H). UV−vis (THF) λ_{max}/nm (ε/M^{-1} cm^{-1}): 472 (4,960), 621 (10,200). MS (ESI−) m/z: 567.1 ($[M]^{1-}$).

Reduction of K[V(SNS)$_2$]. In a 100 mL Schlenk flask, to a chilled blue solution of K[V(SNS)$_2$] (65 mg, 0.073 mmol, 1.00 equiv) in THF (∼10 mL) was added freshly prepared potassium graphite (10 mg, 0.077 mmol, 1.05 equiv). The solution was warmed to room temperature and stirred for ∼1 h. The resulting dark-green solution was filtered through a plug of Celite, and the solvent was removed under reduced pressure to afford putative K$_2$[V(SNS)$_2$].

Synthesis of [K(18-Crown-6) (THF)$_2$][V(SNS)$_2${Ni(dppe)}$_2$]. A 100 mL Schlenk flask containing potassium graphite [102 mg, 0.75 mmol, 5.01 equiv (excess)] was charged with a blue solution containing K[V(SNS)$_2$] (135 mg, 0.151 mmol, 1.00 equiv) dissolved in 20 mL of dry, degassed THF. The color of the reaction mixture initially changes to dark green, indicative of the $[V(SNS)_2]^{2-}$ dianion, followed by a change to brown black. This brown−black reaction mixture was frozen in a liquid-nitrogen cold well. The reaction mixture was removed from the cold well, and upon thawing, a suspension of $NiCl_2$(dppe) (159 mg, 0.301 mmol, 2.00 equiv) in THF (∼10 mL) was added. The mixture was allowed to warm to ambient glovebox temperature and was stirred for 8 h. The resulting vibrant-green solution was filtered through a plug of Celite, and 18-crown-6 (44 mg, 0.17 mmol, 1.0 equiv) was added to the filtrate. The filtrate volume was reduced to approximately 2 mL under reduced pressure, and then, pentane was added to induce precipitation. A dark-green solid was collected by filtration, washed sequentially with 20 mL of pentane and 20 mL of diethyl ether, and dried under reduced pressure to afford 205 mg of the product (70% yield). ^1H NMR (500 MHz, 208 K, THF-d_8): δ/ppm: 2.09 (s, 12H, CH_3), 6−8 (m, 52H, aryl−H). $^{31}P\{^1H\}$ NMR (162 MHz, 208 K, THF-d_8) δ/ppm: 44.6 (s). UV-vis-NIR (THF) λ_{max}/nm (ε/M^{-1} cm^{-1}): 353 nm (31,200), 631 nm (4700). MS (ESI−) m/z: 1479.2 ($[M]^{1-}$).

Synthesis of V(SNS)$_2${Ni(dppe)}$_2$. The neutral trimetallic complex was prepared using the same procedure as that mentioned above but with three equivalents of potassium graphite instead of four. Thus, in a 100 mL Schlenk flask charged with potassium graphite (21 mg of potassium metal, 0.54 mmol, 3.2 equiv) was added a blue solution of K[V(SNS)$_2$] (152 mg, 0.170 mmol, 1.00 equiv.) in THF (∼10 mL), and $NiCl_2$(dppe) (180 mg, 0.340 mmol, 2.00 equiv) afforded 170 mg of the product as a green powder (67% yield). Anal. calcd (Found) for $C_{80}H_{72}N_2Ni_2P_4S_4V$ (%): C, 64.84 (64.62); H, 4.90 (4.88); N, 1.89 (2.02). UV-vis-NIR (THF) λ_{max}/nm (ε/M^{-1} cm^{-1}): 410 nm (14,300), 627 nm (6000). MS (ESI+) m/z: 1480.2 ($[M + H]^{1+}$).

■ ASSOCIATED CONTENT

Supporting Information

The Supporting Information is available free of charge at https://pubs.acs.org/doi/10.1021/acs.inorgchem.2c03381.

Full experimental and crystallographic details and additional spectroscopic and computational data (PDF)

Accession Codes

CCDC 2203724−2203726 contain the supplementary crystallographic data for this paper. These data can be obtained free of charge via www.ccdc.cam.ac.uk/data_request/cif, or by emailing data_request@ccdc.cam.ac.uk, or by contacting The

https://doi.org/10.1021/acs.inorgchem.2c03381
Inorg. Chem. 2023, 62, 1405−1413

Cambridge Crystallographic Data Centre, 12 Union Road, Cambridge CB2 1EZ, U.K.; fax: +44 1223 336033.

AUTHOR INFORMATION

Corresponding Author

Alan F. Heyduk − *Department of Chemistry, University of California at Irvine, Irvine, California 92677-2025, United States;* orcid.org/0000-0003-2183-7099; Email: aheyduk@uci.edu

Authors

Michael K. Wojnar − *Department of Chemistry, University of California at Irvine, Irvine, California 92677-2025, United States;* orcid.org/0000-0003-2556-7014

Joseph W. Ziller − *Department of Chemistry, University of California at Irvine, Irvine, California 92677-2025, United States;* orcid.org/0000-0001-7404-950X

Complete contact information is available at: https://pubs.acs.org/10.1021/acs.inorgchem.2c03381

Notes

The authors declare no competing financial interest.

ACKNOWLEDGMENTS

This work was funded by the National Science Foundation (CHE-1800386). The authors thank Dr. Claudia Ramirez and Dr. Bronte Charette for all of the support. The authors thank Prof. Andy Borovik for EPR spectrometer use.

REFERENCES

(1) Gamelin, D. R.; Bominaar, E. L.; Kirk, M. L.; Wieghardt, K.; Solomon, E. I. Excited-State Contributions to Ground-State Properties of Mixed-Valence Dimers: Spectral and Electronic-Structural Studies of $[Fe_2(OH)_3(tmtacn)_2]^{2+}$ Related to the $[Fe_2S_2]^+$ Active Sites of Plant-Type Ferredoxins. *J. Am. Chem. Soc.* **1996**, *118*, 8085−8097.

(2) Bechlars, B.; D'Alessandro, D. M.; Jenkins, D. M.; Iavarone, A. T.; Glover, S. D.; Kubiak, C. P.; Long, J. R. High-Spin Ground States via Electron Delocalization in Mixed-Valence Imidazolate-Bridged Divanadium Complexes. *Nat. Chem.* **2010**, *2*, 362−368.

(3) Park, J. G.; Collins, B. A.; Darago, L. E.; Runčevski, T.; Ziebel, M. E.; Aubrey, M. L.; Jiang, H. Z. H.; Velasquez, E.; Green, M. A.; Goodpaster, J. D.; Long, J. R. Magnetic Ordering through Itinerant Ferromagnetism in a Metal−Organic Framework. *Nat. Chem.* **2021**, *13*, 594−598.

(4) Zener, C. Interaction between the d-Shells in the Transition Metals. II. Ferromagnetic Compounds of Manganese with Perovskite Structure. *Phys. Rev.* **1951**, *82*, 403−405.

(5) Hua, C.; Doheny, P. W.; Ding, B.; Chan, B.; Yu, M.; Kepert, C. J.; D'Alessandro, D. M. Through-Space Intervalence Charge Transfer as a Mechanism for Charge Delocalization in Metal−Organic Frameworks. *J. Am. Chem. Soc.* **2018**, *140*, 6622−6630.

(6) Chakarawet, K.; Atanasov, M.; Marbey, J.; Bunting, P. C.; Neese, F.; Hill, S.; Long, J. R. Strong Electronic and Magnetic Coupling in M_4 (M = Ni, Cu) Clusters via Direct Orbital Interactions between Low-Coordinate Metal Centers. *J. Am. Chem. Soc.* **2020**, *142*, 19161−19169.

(7) Carter, C.; Kratish, Y.; Jurca, T.; Gao, Y.; Marks, T. J. Bis-Ferrocenyl-Pyridinediimine Trinuclear Mixed-Valent Complexes with Metal-Binding Dependent Electronic Coupling: Synthesis, Structures, and Redox-Spectroscopic Characterization. *J. Am. Chem. Soc.* **2020**, *142*, 18715−18729.

(8) Kirk, M. L.; Shultz, D. A.; Schmidt, R. D.; Habel-Rodriguez, D.; Lee, H.; Lee, J. Ferromagnetic Nanoscale Electron Correlation Promoted by Organic Spin-Dependent Delocalization. *J. Am. Chem. Soc.* **2009**, *131*, 18304−18313.

(9) Porter, T. M.; Heim, G. P.; Kubiak, C. P. Stable Mixed-Valent Complexes Formed by Electron Delocalization Across Hydrogen Bonds of Pyrimidinone-Linked Metal Clusters. *J. Am. Chem. Soc.* **2018**, *140*, 12756−12759.

(10) Robin, M. B.; Day, P. Mixed Valence Chemistry-A Survey and Classification. *Adv. Inorg. Chem. Radiochem.* **1968**, *10*, 247−422.

(11) Glover, S. D.; Goeltz, J. C.; Lear, B. J.; Kubiak, C. P. Inter- or Intramolecular Electron Transfer between Triruthenium Clusters: We'll Cross That Bridge When We Come to It. *Coord. Chem. Rev.* **2010**, *254*, 331−345.

(12) Kubiak, C. P. Inorganic Electron Transfer: Sharpening a Fuzzy Border in Mixed Valency and Extending Mixed Valency across Supramolecular Systems. *Inorg. Chem.* **2013**, *52*, 5663−5676.

(13) Bartholomew, A. K.; Teesdale, J. J.; Hernández Sánchez, R.; Malbrecht, B. J.; Juda, C. E.; Ménard, G.; Bu, W.; Iovan, D. A.; Mikhailine, A. A.; Zheng, S.-L.; Sarangi, R.; Wang, S. G.; Chen, Y.-S.; Betley, T. A. Exposing the Inadequacy of Redox Formalisms by Resolving Redox Inequivalence within Isovalent Clusters. *Proc. Natl. Acad. Sci.* **2019**, *116*, 15836−15841.

(14) Allen, G. C.; Hush, N. S. Intervalence-Transfer Absorption. Part 1. Qualitative Evidence for Intervalence-Transfer Absorption in Inorganic Systems in Solution and in the Solid State. *Prog. Inorg. Chem.* **1967**, *8*, 357−389.

(15) Hush, N. S. Intervalence-Transfer Absorption. Part 2. Theoretical Considerations and Spectroscopic Data. *Prog. Inorg. Chem.* **1967**, *8*, 391−444.

(16) Nocera, D. G. Chemistry of the Multielectron Excited State. *Acc. Chem. Res.* **1995**, *28*, 209−217.

(17) Esswein, A. J.; Nocera, D. G. Hydrogen Production by Molecular Photocatalysis. *Chem. Rev.* **2007**, *107*, 4022−4047.

(18) Heyduk, A. F.; Nocera, D. G. A Novel Two-Electron Mixed-Valence Ir(II)−Ir(0) Complex. *Chem. Commun.* **1999**, 1519−1520.

(19) Heyduk, A. F.; Nocera, D. G. Hydrido, Halo, and Hydrido-Halo Complexes of Two-Electron Mixed-Valence Diiridium Cores. *J. Am. Chem. Soc.* **2000**, *122*, 9415−9426.

(20) Heyduk, A. F.; Nocera, D. G. Hydrogen Produced from Hydrohalic Acid Solutions by a Two-Electron Mixed-Valence Photocatalyst. *Science* **2001**, *293*, 1639−1641.

(21) Gray, T. G.; Veige, A. S.; Nocera, D. G. Cooperative Bimetallic Reactivity: Hydrogen Activation in Two-Electron Mixed-Valence Compounds. *J. Am. Chem. Soc.* **2004**, *126*, 9760−9768.

(22) Veige, A. S.; Nocera, D. G. Water Addition to a Two-Electron Mixed-Valence Bimetallic Center. *Chem. Commun.* **2004**, 1958−1959.

(23) Gray, T. G.; Nocera, D. G. A Model for Two-Electron Mixed Valence in Metal−Metal Bonded Dirhodium Compounds. *Chem. Commun.* **2005**, 1540−1542.

(24) Esswein, A. J.; Veige, A. S.; Nocera, D. G. A Photocycle for Hydrogen Production from Two-Electron Mixed-Valence Complexes. *J. Am. Chem. Soc.* **2005**, *127*, 16641−16651.

(25) Dempsey, J. L.; Esswein, A. J.; Manke, D. R.; Rosenthal, J.; Soper, J. D.; Nocera, D. G. Molecular Chemistry of Consequence to Renewable Energy. *Inorg. Chem.* **2005**, *44*, 6879−6892.

(26) Veige, A. S.; Gray, T. G.; Nocera, D. G. Hydrogenation of Two-Electron Mixed-Valence Iridium Alkyl Complexes. *Inorg. Chem.* **2005**, *44*, 17−26.

(27) Esswein, A. J.; Veige, A. S.; Piccoli, P. M. B.; Schultz, A. J.; Nocera, D. G. Intramolecular C−H Bond Activation and Redox Isomerization across Two-Electron Mixed Valence Diiridium Cores. *Organometallics* **2008**, *27*, 1073−1083.

(28) Teets, T. S.; Cook, T. R.; McCarthy, B. D.; Nocera, D. G. Redox Chemistry, Acid Reactivity, and Hydrogenation Reactions of Two-Electron Mixed Valence Diiridium and Dirhodium Complexes. *Inorg. Chem.* **2011**, *50*, 5223−5233.

(29) Teets, T. S.; Cook, T. R.; McCarthy, B. D.; Nocera, D. G. Oxygen Reduction to Water Mediated by a Dirhodium Hydrido-Chloride Complex. *J. Am. Chem. Soc.* **2011**, *133*, 8114−8117.

(30) Powers, D. C.; Hwang, S. J.; Zheng, S.-L.; Nocera, D. G. Halide-Bridged Binuclear HX-Splitting Catalysts. *Inorg. Chem.* **2014**, *53*, 9122−9128.

(31) Chambers, G. M.; Angamuthu, R.; Gray, D. L.; Rauchfuss, T. B. Organo Ruthenium−Nickel Dithiolates with Redox-Responsive Nickel Sites. *Organometallics* **2013**, *32*, 6324−6329.
(32) Chambers, G. M.; Mitra, J.; Rauchfuss, T. B.; Stein, M. Ni^{I}/Ru^{II} Model for the Ni−L State of the [NiFe] Hydrogenases: Synthesis, Spectroscopy, and Reactivity. *Inorg. Chem.* **2014**, *53*, 4243−4249.
(33) Heyduk, A. F.; Macintosh, A. M.; Nocera, D. G. Four-Electron Photochemistry of Dirhodium Fluorophosphine Compounds. *J. Am. Chem. Soc.* **1999**, *121*, 5023−5032.
(34) Shaffer, D. W.; Szigethy, G.; Ziller, J. W.; Heyduk, A. F. Synthesis and Characterization of a Redox-Active Bis(Thiophenolato)Amide Ligand, $[SNS]^{3-}$, and the Homoleptic Tungsten Complexes, $W[SNS]_2$ and $W[ONO]_2$. *Inorg. Chem.* **2013**, *52*, 2110−2118.
(35) Rosenkoetter, K. E.; Wojnar, M. K.; Charette, B. J.; Ziller, J. W.; Heyduk, A. F. Hydrogen-Atom Noninnocence of a Tridentate [SNS] Pincer Ligand. *Inorg. Chem.* **2018**, *57*, 9728−9737.
(36) Charette, B. J.; Ziller, J. W.; Heyduk, A. F. Metal-Ion Influence on Ligand-Centered Hydrogen-Atom Transfer. *Inorg. Chem.* **2021**, *60*, 1579−1589.
(37) Herebian, D.; Bothe, E.; Bill, E.; Weyhermüller, T.; Wieghardt, K. Experimental Evidence for the Noninnocence of *o*-Aminothiophenolates: Coordination Chemistry of *o*-Iminothionebenzosemiquinonate(1-) π-Radicals with Ni(II), Pd(II), Pt(II). *J. Am. Chem. Soc.* **2001**, *123*, 10012−10023.
(38) Sproules, S.; Wieghardt, K. Dithiolene Radicals: Sulfur K-Edge X-Ray Absorption Spectroscopy and Harry's Intuition. *Coord. Chem. Rev.* **2011**, *255*, 837−860.
(39) Ghosh, P.; Begum, A.; Herebian, D.; Bothe, E.; Hildenbrand, K.; Weyhermüller, T.; Wieghardt, K. Coordinated *o*-Dithio- and *o*-Iminothiobenzosemiquinonate(1−) π Radicals in $[M^{II}(Bpy)(L^{\cdot})](PF_6)$ Complexes. *Angew. Chem., Int. Ed.* **2003**, *42*, 563−567.
(40) Sproules, S.; Banerjee, P.; Weyhermüller, T.; Yan, Y.; Donahue, J. P.; Wieghardt, K. Monoanionic Molybdenum and Tungsten Tris(Dithiolene) Complexes: A Multifrequency EPR Study. *Inorg. Chem.* **2011**, *50*, 7106−7122.
(41) Roy, N.; Sproules, S.; Weyhermüller, T.; Wieghardt, K. Trivalent Iron and Ruthenium Complexes with a Redox Noninnocent (2-Mercaptophenylimino)-Methyl-4,6-Di-*Tert*-Butylphenolate(2-) Ligand. *Inorg. Chem.* **2009**, *48*, 3783−3791.
(42) Pauling, L. Atomic Radii and Interatomic Distances in Metals. *J. Am. Chem. Soc.* **1947**, *69*, 542−553.
(43) Cordero, B.; Gómez, V.; Platero-Prats, A. E.; Revés, M.; Echeverría, J.; Cremades, E.; Barragán, F.; Alvarez, S. Covalent Radii Revisited. *Dalton Trans.* **2008**, 2832−2838.
(44) Eichhöfer, A.; Andrushko, V.; Bodenstein, T.; Fink, K. Trinuclear Early/Late-Transition-Metal Thiolate Complexes. *Eur. J. Inorg. Chem.* **2014**, 3510−3520.
(45) Clouston, L. J.; Bernales, V.; Cammarota, R. C.; Carlson, R. K.; Bill, E.; Gagliardi, L.; Lu, C. C. Heterobimetallic Complexes That Bond Vanadium to Iron, Cobalt, and Nickel. *Inorg. Chem.* **2015**, *54*, 11669−11679.
(46) Wu, B.; Wilding, M. J. T.; Kuppuswamy, S.; Bezpalko, M. W.; Foxman, B. M.; Thomas, C. M. Exploring Trends in Metal−Metal Bonding, Spectroscopic Properties, and Conformational Flexibility in a Series of Heterobimetallic Ti/M and V/M Complexes (M = Fe, Co, Ni, and Cu). *Inorg. Chem.* **2016**, *55*, 12137−12148.
(47) Huynh, M. T.; Schilter, D.; Hammes-Schiffer, S.; Rauchfuss, T. B. Protonation of Nickel−Iron Hydrogenase Models Proceeds after Isomerization at Nickel. *J. Am. Chem. Soc.* **2014**, *136*, 12385−12395.
(48) Schilter, D.; Rauchfuss, T. B.; Stein, M. Connecting [NiFe]- and [FeFe]-Hydrogenases: Mixed-Valence Nickel-Iron Dithiolates with Rotated Structures. *Inorg. Chem.* **2012**, *51*, 8931−8941.
(49) Chu, X.; Xu, X.; Su, H.; Raje, S.; Angamuthu, R.; Tung, C.-H.; Wang, W. Heteronuclear Assembly of Ni−Cu Dithiolato Complexes: Synthesis, Structures, and Reactivity Studies. *Inorg. Chem. Front.* **2017**, *4*, 706−711.
(50) Chu, X.; Jin, J.; Ming, B.; Pang, M.; Yu, X.; Tung, C.-H.; Wang, W. Bimetallic Nickel−Cobalt Hydrides in H_2 Activation and Catalytic Proton Reduction. *Chem. Sci.* **2019**, *10*, 761−767.
(51) Sproules, S.; Weyhermüller, T.; DeBeer, S.; Wieghardt, K. Six-Membered Electron Transfer Series $[V(Dithiolene)_3]^z$ (z = 1+, 0, 1−, 2−, 3−, 4−). An X-Ray Absorption Spectroscopic and Density Functional Theoretical Study. *Inorg. Chem.* **2010**, *49*, 5241−5261.
(52) Zadrozny, J. M.; Niklas, J.; Poluektov, O. G.; Freedman, D. E. Millisecond Coherence Time in a Tunable Molecular Electronic Spin Qubit. *ACS Cent. Sci.* **2015**, *1*, 488−492.
(53) Fataftah, M. S.; Krzyaniak, M. D.; Vlaisavljevich, B.; Wasielewski, M. R.; Zadrozny, J. M.; Freedman, D. E. Metal−Ligand Covalency Enables Room Temperature Molecular Qubit Candidates. *Chem. Sci.* **2019**, *10*, 6707−6714.
(54) Wojnar, M. K.; Ziller, J. W.; Heyduk, A. F. Heterobimetallic and Heterotrimetallic Clusters Containing a Redox-Active Metalloligand. *Eur. J. Inorg. Chem.* **2017**, *2017*, 5571−5575.
(55) Wong, J. L.; Higgins, R. F.; Bhowmick, I.; Cao, D. X.; Szigethy, G.; Ziller, J. W.; Shores, M. P.; Heyduk, A. F. Bimetallic Iron−Iron and Iron−Zinc Complexes of the Redox-Active ONO Pincer Ligand. *Chem. Sci.* **2016**, *7*, 1594−1599.
(56) Rosenkoetter, K. E.; Ziller, J. W.; Heyduk, A. F. A Heterobimetallic W−Ni Complex Containing a Redox-Active W-$[SNS]_2$ Metalloligand. *Inorg. Chem.* **2016**, *55*, 6794−6798.
(57) Rosenkoetter, K. E.; Ziller, J. W.; Heyduk, A. F. Heterobimetallic Complexes of Palladium and Platinum Containing a Redox-Active $W[SNS]_2$ Metalloligand. *Dalton Trans.* **2017**, *46*, 5503−5507.
(58) Miedaner, A.; Haltiwanger, R. C.; DuBois, D. L. Relationship between the Bite Size of Diphosphine Ligands and Tetrahedral Distortions of "Square-Planar" Nickel(II) Complexes: Stabilization of Nickel(I) and Palladium(I) Complexes Using Diphosphine Ligands with Large Bites. *Inorg. Chem.* **1991**, *30*, 417−427.
(59) Ulloa, O. A.; Huynh, M. T.; Richers, C. P.; Bertke, J. A.; Nilges, M. J.; Hammes-Schiffer, S.; Rauchfuss, T. B. Mechanism of H_2 Production by Models for the [NiFe]-Hydrogenases: Role of Reduced Hydrides. *J. Am. Chem. Soc.* **2016**, *138*, 9234−9245.
(60) Basu, D.; Bailey, T. S.; Lalaoui, N.; Richers, C. P.; Woods, T. J.; Rauchfuss, T. B.; Arrigoni, F.; Zampella, G. Synthetic Designs and Structural Investigations of Biomimetic Ni−Fe Thiolates. *Inorg. Chem.* **2019**, *58*, 2430−2443.
(61) Britt, R. D.; Rao, G.; Tao, L. Bioassembly of Complex Iron−Sulfur Enzymes: Hydrogenases and Nitrogenases. *Nat. Rev. Chem.* **2020**, *4*, 542−549.
(62) Britto, S.; Leskes, M.; Hua, X.; Hébert, C.-A.; Shin, H. S.; Clarke, S.; Borkiewicz, O.; Chapman, K. W.; Seshadri, R.; Cho, J.; Grey, C. P. Multiple Redox Modes in the Reversible Lithiation of High-Capacity, Peierls-Distorted Vanadium Sulfide. *J. Am. Chem. Soc.* **2015**, *137*, 8499−8508.
(63) Manxzer, L. E.; Deaton, J.; Sharp, P.; Schrock, R. R. Tetrahydrofuran Complexes of Selected Early Transition Metals. *Inorg. Synth.* **1982**, 135−140.
(64) Standley, E. A.; Smith, S. J.; Müller, P.; Jamison, T. F. A Broadly Applicable Strategy for Entry into Homogeneous Nickel(0) Catalysts from Air-Stable Nickel(II) Complexes. *Organometallics* **2014**, *33*, 2012−2018.

https://doi.org/10.1021/acs.inorgchem.2c03381
Inorg. Chem. 2023, 62, 1405−1413